

Bayesian De-quantization and Data Compression for Low-Energy Physiological Signal Telemonitoring

Benyuan Liu*, *Student Member, IEEE*, Hongqi Fan, and Qiang Fu, Zhilin Zhang, *Member, IEEE*

Abstract—We address the issue of applying quantized compressed sensing (CS) on low-energy telemonitoring. So far, few works studied this problem in applications where signals were only approximately sparse. We propose a two-stage data compressor based on quantized CS, where signals are compressed by compressed sensing and then the compressed measurements are quantized with only 2 bits per measurement. This compressor can greatly reduce the transmission bit-budget. To recover signals from underdetermined, quantized measurements, we develop a Bayesian De-quantization algorithm. It can exploit both the model of quantization errors and the correlated structure of physiological signals to improve the quality of recovery. The proposed data compressor and the recovery algorithm are validated on a dataset recorded on 12 subjects during fast running. Experiment results showed that an averaged 2.596 beat per minute (BPM) estimation error was achieved by jointly using compressed sensing with 50% compression ratio and a 2-bit quantizer. The results imply that we can effectively transmit n bits instead of n samples, which is a substantial improvement for low-energy wireless telemonitoring.

Index Terms—Quantized Compressed Sensing, Block Sparse Bayesian Learning, Data Compression, Telemonitoring

I. INTRODUCTION

In wireless health monitoring systems [1], large amount and various types of physiological signals are collected from on-body sensors, and then transmitted to nearby smart-phones or data central via wireless networks. Energy consumption is a critical issue in these systems. Compressed sensing (CS) [2] is a promising technique for such systems for low-energy data acquisition, compression, and wireless transmission [3], [4].

In the framework of CS, a signal $\mathbf{x} \in \mathbb{R}^N$ is compressed by a simple matrix-vector multiplication,

$$\mathbf{y} = \Phi \mathbf{x} + \mathbf{n}. \quad (1)$$

where $\Phi \in \mathbb{R}^{M \times N}$ is called the sensing matrix, $\mathbf{y} \in \mathbb{R}^M$ is the compressed measurements and \mathbf{n} is the measurement noise. Usually Φ is underdetermined, i.e., $M < N$, and the ratio $(N - M)/N$ is called the compression ratio of CS.

Asterisk indicates corresponding author.

*B. Liu is with The Science and Technology on Automatic Target Recognition Laboratory, National University of Defense Technology, Changsha, Hunan 410074, China and also with the Department of Biomedical Engineering, Fourth Military Medical University, Xi'an 710032, China. (e-mail: byliu@fmmu.edu.cn)

H.-Q. Fan, Q. Fu are with The Science and Technology on Automatic Target Recognition Laboratory, National University of Defense Technology, Changsha, Hunan, 410074, China (e-mail: {fanhongqi,fq}@nudt.edu.cn)

Z. Zhang is with The Emerging Technology Lab, Samsung Research America - Dallas, 1301 East Lookout Drive, Richardson, TX 75082, USA. (e-mail: zhilinzhang@ieee.org)

Manuscript received June 9, 2015.

Compression via CS can be implemented in two ways as shown in Fig. 1. One is analog CS [5]–[8], where the matrix-vector multiplication $\Phi \mathbf{x}$ is implemented in analog domain and the compressed measurements are quantized via an Analog-to-Digital Converter (ADC). Analog CS is also called Analog-to-Information Converter (AIC) [7], [8]. Usually, an AIC is implemented in a dedicate ASIC chip to achieve low-energy. The other is digital CS, where signals are firstly quantized into digitalized samples and $\Phi \mathbf{x}$ is calculated in MCU [9] or FPGA [10]. The advantage of digital CS is that it can utilize exiting ADCs and can be implemented as an efficient, low-energy data compressor [10]. In both cases, the sensing matrix Φ needs

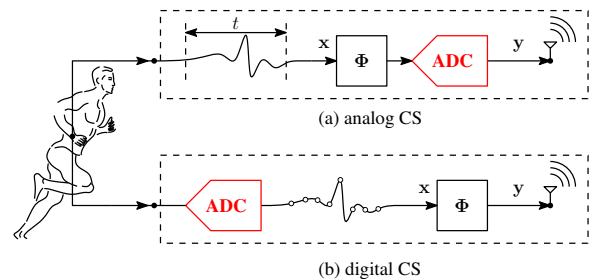


Fig. 1. Compression via Compressed Sensing (CS). The matrix-vector multiplication in (1) can be either implemented using analog circuit in (a) or digitally in (b). In both cases, an ADC is required to convert continuous signals to quantized numbers.

not to be transmitted and is stored in both the transmitter and receiver.

At a receiver, the original signal \mathbf{x} is recovered from the compressed measurements \mathbf{y} via

$$\min \|\mathbf{x}\|_0 \quad \text{subject to} \quad \|\mathbf{y} - \Phi \mathbf{x}\|_2 \leq \varepsilon \quad (2)$$

where $\|\mathbf{x}\|_0$ is the ℓ_0 norm of $\|\mathbf{x}\|$, and ε is the tolerance of noise or modeling errors. Calculating the solution is very hard. Generally, one seeks the solution of a relaxed convex optimization problem [11], in which $\|\mathbf{x}\|_0$ is replaced by $\|\mathbf{x}\|_1$ or other terms encouraging sparse solutions. The quality of signal recovery can be improved by exploiting other structure information in signals, such as wavelet-tree structure [12], piecewise smooth [13] or block sparse structure [3], [14].

CS has been successfully used in low-energy telemonitoring of physiological signals such as EEG [15] or fetal ECG [3]. However, these works [3], [15] assumed that the compressed measurements \mathbf{y} was real-valued. But in practice, the compressed measurements \mathbf{y} must be quantized before transmission, i.e.,

$$\mathbf{y} = \mathcal{Q}(\Phi \mathbf{x}) \quad (3)$$

where $\mathcal{Q}(\cdot)$ is the quantization operator that maps a real-valued signal to finite quantization levels [16]. This process unavoidably introduces errors, called quantization errors. Some CS algorithms [17]–[19] were developed to recover signals from the quantized measurements. This recovery procedure is often called de-quantization [20] and a CS algorithm is also called a decoder [21]. Haboba *et al.* studied the quantization errors and its effect on signal recovery using synthetic signals with fixed sparsity [7]. However, the signal model used in [7] is not practical for telemonitoring applications, as most physiological signals are only approximately sparse. Wang *et al.* analyzed the performance-to-energy trade-offs introduced by quantized CS [8] in EEG telemonitoring and provided a brute force method searching the optimum configuration of the quantizer. But the CS algorithm used in [8] ignored the model of quantization errors during signal recovery, which may yield degraded performance.

Although quantization introduces errors, suitably using quantization can largely reduce the wireless transmission bit-budget [22]. In this work, we address this issue and use quantized CS for low-energy telemonitoring. First, physiological signals are compressed according to (1), and then quantized according to (3) with 2 bits per measurement. This compression scheme greatly reduces the transmission bit-budget, which benefits to low-energy telemonitoring.

On the de-compression and de-quantization stage, we propose a Bayesian de-quantization algorithm, denoted by BDQ. It exploits correlation structure within physiological signals and also takes into account the quantization errors. Note that this algorithm does not exploit sparsity to recover signals, as done by most other compressed sensing algorithms. Instead, it exploits correlation of physiological signals. Our motivation is that during wireless health monitoring many raw physiological signals are usually less sparse, namely these noisy signals are not sparse in the time domain and also not sparse in other transform domains [23]. In this case exploiting sparsity may not be very effective. In contrast, exploiting correlation may be a better direction, as shown in [3]. However, the work in [3] did not consider the quantization errors, and thus has inferior performance to our proposed BDQ algorithm, as shown in experiments later.

We study the application of Photoplethysmography (PPG) and accelerometer telemonitoring for fitness training, in which the heart rate must be accurately estimated during intensive physical exercises. We exploit the optimum compression by jointly tuning the compression ratio (CR) of CS and the quantization bit-depth. The experiment results show that an averaged 2.596 BPM absolute heart rate estimation error is achieved with CR = 0.50 and a 2 bits quantizer. The Pearson correlation between the estimated heart rate from the recovered datasets and the ground-truth is 0.9899. These results imply that we can effectively compress raw segments of PPG and accelerometer data from N samples into N bits for low-energy telemonitoring.

The rest of the paper is organized as follows. Section II introduces the quantization model of compressed sensing. The Bayesian De-Quantize algorithm are presented and discussed in Section III. Section IV describes the experimental set up

and numerical results. Discussions are given in Section V and Section VI concludes the paper.

II. THE QUANTIZATION MODEL OF COMPRESSED SENSING

The function of an ADC is *time* sampling and *scale* quantization, which is illustrated in Fig. 2. Let B denotes the number

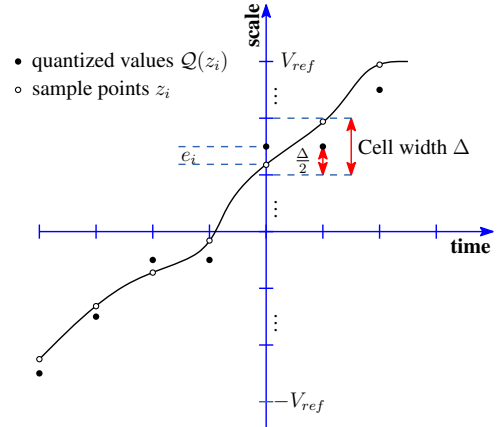


Fig. 2. Time sampling and scale quantization. The quantization error is denoted by e_i and the cell width is Δ . The mid-point value within a cell is taken as the quantized value for a sample point falling in that cell.

of bits per measurement, which is also called the bit-depth of a quantizer. Represented by B bits, the scales between the positive and negative reference voltage $[-V_{ref}, V_{ref}]$ are divided into $L = 2^B$ quantization levels. The cell width [16] Δ of a uniform quantizer is

$$\Delta = \frac{2V_{ref}}{2^B}. \quad (4)$$

Signals larger than V_{ref} or smaller than $-V_{ref}$ are saturated. Those saturation signals are quantized with the same level as signals lie in $[V_{ref} - \Delta, V_{ref}]$ or $[-V_{ref} + \Delta, -V_{ref}]$.

For a sample $v_i \in \mathbb{R}$ falls in a cell, the mid-point value in that cell is used as the quantization value $\mathcal{Q}(v_i)$. The quantization error e_i is defined as

$$e_i = \mathcal{Q}(v_i) - v_i, \quad (5)$$

e_i distributes uniformly between $[-\Delta/2, \Delta/2]$. Let $\mathcal{D}_e = [-\Delta/2, \Delta/2]$ denotes the domain of quantization errors, then

$$p(e_i) \sim \mathcal{U}(\mathcal{D}_e). \quad (6)$$

It should be noted that \mathcal{D}_e is unbounded when a signal saturates [19]. Furthermore, the variance of the quantization error, denoted by σ_e , is,

$$\sigma_e = \frac{\Delta^2}{12}. \quad (7)$$

A. Analog CS

For analog CS, the matrix-vector multiplication $\Phi \mathbf{x}$ is implemented in analog domain and the compressed measurements are quantized via an ADC before transmission,

$$\mathbf{y} = \Phi \mathbf{x} + \mathbf{n}, \quad \mathbf{y}_q = \mathcal{Q}(\mathbf{y}) \quad (8)$$

where the subscript q denote the quantized signals. Let $\mathbf{e} = \mathbf{y}_q - \mathbf{y}$, we have,

$$\mathbf{y}_q = \Phi \mathbf{x} + \mathbf{n} + \mathbf{e}. \quad (9)$$

The transmission bit-budget of analog CS is MB bits, which can be controlled by the number of compressed measurements M as well as the quantization bit-depth B of the ADC.

B. Digital CS

For digital CS, analog signals are firstly quantized by an ADC via Nyquist sampling, then the digitalized signals are compressed in MCU [9] or FPGA [10] via a matrix-vector multiplication,

$$\mathbf{y} = \Phi \mathbf{x}_q + \mathbf{n}, \quad \mathbf{x}_q = Q(\mathbf{x}) \quad (10)$$

In practice, larger bit-depth B_i is required for the ADC to reduce the distortions during signal acquisition (i.e., $B_i = 12$ was used in [10]). For larger B_i , the variance of the quantization error \mathbf{e} is much smaller and (10) is simplified as,

$$\mathbf{y} = \Phi \mathbf{x}_q + \mathbf{n}, \quad \mathbf{x}_q \approx \mathbf{x} \quad (11)$$

C. The two-stage data compressor

In (10), both \mathbf{y} and \mathbf{x}_q are represented in fixed-point arithmetic with B_i bits [10]. We may further reduce transmission bit-budget by simply rounding each sample of \mathbf{y} to B bits, denoted by $\mathbf{y}_q = Q_r(\mathbf{y})$, where $Q_r(\cdot)$ is called a rounding

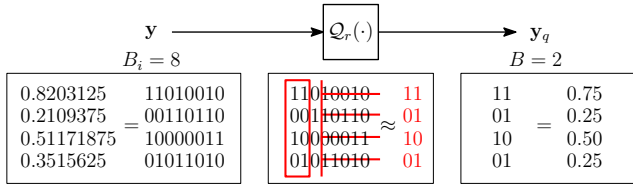


Fig. 3. The operator $Q_r(\cdot)$ can be efficiently implemented in digital CS. In this example, the compressed measurements \mathbf{y} are represented using unsigned fix-point arithmetic ($B_i = 8$ and the fraction length is also 8 bits). The rounding outputs \mathbf{y}_q have only 2 bits per sample.

operator and its function is illustrated in Fig. 3. Q_r can be regarded as an economy quantizer in fixed-point arithmetic.

We denote by $\mathbf{e}_r = \mathbf{y}_q - \mathbf{y}$ the rounding error, which assumed to be uniform distributed,

$$p(\mathbf{e}_r) \sim \mathcal{U}(\mathcal{D}_{e_r}) \quad (12)$$

where $\mathcal{D}_{e_r} = [-\Delta_r/2, \Delta_r/2]$ and the cell width $\Delta_r = \frac{2V_{ref}}{2^B}$. After rounding, (11) can be reformulated as,

$$\mathbf{y}_q = \Phi \mathbf{x}_q + \mathbf{n} + \mathbf{e}_r, \quad \mathbf{x}_q \approx \mathbf{x} \quad (13)$$

The bit-compression ratio CR_b , i.e., the ratio between the reduced bit-budget after compression divided by the total input bit-budget, is defined as

$$CR_b = \frac{NB_i - MB}{NB_i} = 1 - (1 - CR) \cdot \frac{B}{B_i} \quad (14)$$

where $CR = (N - M)/N$ is the compression ratio in CS-based telemonitoring [3], [10].

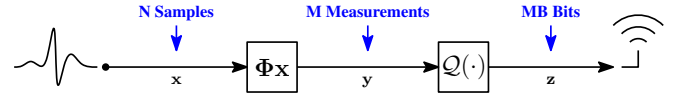


Fig. 4. A unified framework for low-energy wireless telemonitoring using quantized compressed sensing.

In our paper thereafter, we do not distinguish between quantization $Q(\cdot)$ in analog CS (9) and rounding $Q_r(\cdot)$ in digital CS (13). Instead, we model them in a unified framework in Fig. 4, which is a two-stage data compressor that can be formulated as,

$$\mathbf{z} = \Phi \mathbf{x} + \mathbf{e} + \mathbf{n} \quad (15)$$

where \mathbf{z} is the quantized measurements represented with B bits per sample, $\Phi \in \mathbb{R}^{M \times N}$ is the sensing matrix, \mathbf{n} and \mathbf{e} are measurement noise and quantization noise respectively. In this framework, we transmit only MB bits instead of N samples for wireless telemonitoring.

III. THE BAYESIAN DE-QUANTIZE ALGORITHM

A. Bayesian Hierarchical Model

1) *Noise Model*: The measurement noise \mathbf{n} is usually assumed Gaussian with variance λ , i.e., $\mathbf{n} \sim \mathcal{N}(\mathbf{0}, \lambda \mathbf{I})$. From (15) we have

$$p(\mathbf{z}|\mathbf{x}, \mathbf{e}; \lambda) = \mathcal{N}(\Phi \mathbf{x} + \mathbf{e}, \lambda \mathbf{I}) \quad (16)$$

The quantization error \mathbf{e} is uniform distributed,

$$p(\mathbf{e}) = \mathcal{U}(\mathcal{D}_e) \quad (17)$$

where $\mathcal{D}_e = [-\Delta/2, \Delta/2]$ and Δ is the cell width of a quantizer. In practice, the cell width Δ is known a priori given B and the reference voltage V_{ref} .

Remark 1: The quantization error models rounding errors between the analog input and the digitalized output. It is non-linear especially for low-resolution ADCs and also depends on the amplitude and frequency of a signal. Exploiting the dependencies between signals and quantization errors may improve the quality of recovery, however it is difficult to do so [19]. To simplify our model, we assume an uniform distributions for \mathbf{e} and do not consider the dependency between the quantization error and the analog input.

Remark 2: We studied only multi-bit ($B \geq 2$) quantized CS and do not consider the extreme case of 1-bit compressed sensing. 1-bit CS may have better recovery performances than multi-bit CS under the same compressed bit-budget MB [18]. However, 1-bit CS loses scale information of signals, which challenges its use in low-energy telemonitoring applications. We refer the reader to the literature on 1-bit compressed sensing [18] for more details.

2) *Signal Model*: We assume a correlated structure within the signal [14] where we model the prior of signal \mathbf{x} as,

$$p(\mathbf{x}|\gamma, \mathbf{P}) = \mathcal{N}(\mathbf{0}, \gamma \mathbf{P}) \quad (18)$$

where γ is a non-negative parameter controlling the variance of the signal \mathbf{x} , \mathbf{P} is a symmetric positive semi-definite matrix modeling the correlation structure of signal \mathbf{x} . The diagonal entries of \mathbf{P} are normalized to 1s during iterative learning.

B. The Bayesian De-Quantization Algorithm

We estimate $\{\mathbf{x}, \mathbf{e}, \lambda, \gamma, \mathbf{P}\}$ using their joint MAP estimator,

$$\begin{aligned} \{\hat{\mathbf{x}}, \hat{\mathbf{e}}, \hat{\lambda}, \hat{\gamma}, \hat{\mathbf{P}}\} &= \arg \max \log p(\mathbf{x}, \mathbf{e}, \lambda, \gamma, \mathbf{P} | \mathbf{z}) \\ &= \arg \max \log p(\mathbf{e} | \mathbf{z}, \mathbf{x}, \lambda, \gamma, \mathbf{P}) \cdot p(\mathbf{x}, \lambda, \gamma, \mathbf{P} | \mathbf{z}) \end{aligned}$$

A nested Expectation Maximization (nest-EM) approach [24], [25] is adopted. The nest-EM is an iterative monotonically convergent method, it consists of an inner and outer EM loop, which is briefly sketched in Fig. 5.

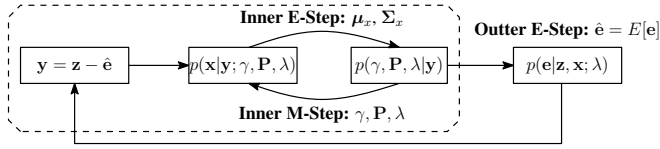


Fig. 5. Bayesian De-Quantization Algorithm using Nested EM approach.

We initialized the nest-EM procedure with $\mathbf{e}_0 = \mathbf{0}$ and let $\mathbf{y} = \mathbf{z} - \mathbf{e}_0$, then iterative over,

- **Inner E-Step**, estimate μ_x and Σ_x from posterior probability $p(\mathbf{x} | \mathbf{y}; \gamma, \mathbf{P}, \lambda)$,
- **Inner M-Step**, update γ , \mathbf{P} and λ via maximize the likelihood $p(\gamma, \mathbf{P}, \lambda | \mathbf{y})$,
- **Outer E-Step**, estimate the first moment of quantization error $\hat{\mathbf{e}}$ from $p(\mathbf{e} | \mathbf{z}, \mathbf{x}; \lambda)$, and update $\mathbf{y} = \mathbf{z} - \hat{\mathbf{e}}$.

1) *Inner-E step*: The posterior $p(\mathbf{x} | \mathbf{y}; \lambda, \gamma, \mathbf{P})$ can be expressed in an analytical form [26],

$$\begin{aligned} p(\mathbf{x} | \mathbf{y}; \lambda, \gamma, \mathbf{P}) &= \frac{p(\mathbf{y} | \mathbf{x}; \lambda) p(\mathbf{x} | \gamma, \mathbf{P})}{p(\mathbf{y} | \lambda, \gamma, \mathbf{P})} \\ &= (2\pi)^{-(N+1)/2} |\Sigma|^{-1/2} \exp \left\{ -\frac{1}{2} (\mathbf{x} - \boldsymbol{\mu})^T \Sigma^{-1} (\mathbf{x} - \boldsymbol{\mu}) \right\}, \end{aligned}$$

where $\boldsymbol{\mu}$ and Σ are respectively,

$$\boldsymbol{\mu} = \gamma \mathbf{P} \boldsymbol{\Phi}^T (\lambda \mathbf{I} + \gamma \boldsymbol{\Phi} \mathbf{P} \boldsymbol{\Phi}^T)^{-1} \mathbf{y} \quad (19)$$

$$\Sigma = \left(\frac{1}{\gamma} \mathbf{P}^{-1} + \frac{1}{\lambda} \boldsymbol{\Phi}^T \boldsymbol{\Phi} \right)^{-1} \quad (20)$$

2) *Inner-M step*: The parameters λ , γ and \mathbf{P} are estimated by a Type II maximum likelihood procedure [26],

$$\mathcal{L}(\lambda, \gamma, \mathbf{P}) = -\log p(\mathbf{y} | \lambda, \gamma, \mathbf{P}) \quad (21)$$

$$= \log |\lambda \mathbf{I} + \gamma \boldsymbol{\Phi} \mathbf{P} \boldsymbol{\Phi}^T| + \mathbf{y}^T (\lambda \mathbf{I} + \gamma \boldsymbol{\Phi} \mathbf{P} \boldsymbol{\Phi}^T)^{-1} \mathbf{y} \quad (22)$$

Optimize over $\mathcal{L}(\lambda, \gamma, \mathbf{P})$, we have update rules for λ , γ and \mathbf{P} respectively,

$$\lambda = \frac{\|\mathbf{y} - \boldsymbol{\Phi} \boldsymbol{\mu}\|_2^2 + \text{Tr}(\Sigma \boldsymbol{\Phi}^T \boldsymbol{\Phi})}{M} \quad (23)$$

$$\mathbf{P} = \frac{\Sigma + \boldsymbol{\mu} \boldsymbol{\mu}^T}{\gamma} \quad (24)$$

$$\gamma = \frac{1}{N} \text{Tr} [\mathbf{P}^{-1} (\Sigma + \boldsymbol{\mu} \boldsymbol{\mu}^T)] \quad (25)$$

Remark 3: Due to the coupling of \mathbf{e} and \mathbf{n} in (15), the estimate of the noise variance λ is inaccurate due to an identifiability issue as stated in [27]. Therefore, λ is often treated as a regularize parameter [10], [19]. We set $\lambda = 0.001$ as the default parameter used in the experiment.

3) *Regularization on P*: Regularization on \mathbf{P} is required due to limited data [14]. In [14], the author provided an empirical method on the regularization of \mathbf{P} using a symmetric Toeplitz matrix,

$$\mathbf{P}_{ij} = r^{|i-j|}, \quad i, j = 1, \dots, N, \quad |r| < 1 \quad (26)$$

where r is the correlation coefficient empirically calculated from the ratio between the mean of sub-diagonal of \mathbf{P} and the mean of main diagonal of \mathbf{P} . Such regularization is equivalent to modeling the correlation structure as a first-order Auto-Regressive (AR) process [27].

An AR(1) matrix has simple tri-diagonal inverse,

$$\mathbf{P}^{-1} = \frac{1}{1-r^2} \begin{pmatrix} 1 & -r & 0 & \dots & 0 \\ -r & 1+r^2 & -r & \dots & 0 \\ \vdots & \ddots & \ddots & \ddots & \vdots \\ 0 & \dots & -r & 1+r^2 & -r \\ 0 & \dots & 0 & -r & 1 \end{pmatrix} \quad (27)$$

and it can be decomposed as

$$\mathbf{P}^{-1} = \frac{1}{1-r^2} \mathbf{T} (\mathbf{D}^T \mathbf{D}) \quad (28)$$

where $\mathbf{T} = \text{diag}\{1, \dots, 1, 1/(1+r^2)\}$ is a diagonal matrix and \mathbf{D} is a temporal smooth operator [28] defined as

$$\mathbf{D} = \begin{pmatrix} 1 & -r & 0 & \dots & 0 \\ 0 & 1 & -r & \dots & 0 \\ & \ddots & \ddots & \ddots & \\ 0 & 0 & \dots & 1 & -r \\ 0 & 0 & \dots & 0 & 1 \end{pmatrix}, \quad (29)$$

A similar regularization method was proposed in [29] which models the inverse covariance matrix as $\mathbf{D}^T \mathbf{D}$.

This type of regularization can exploit the correlated structures within physiological signals [3], [15]. However, the correlation coefficient r in (26) or (29) can only be empirically calculated [14] or fixed [29] in existing algorithms.

We presented in this paper an AR(1) approximation to estimate the correlation matrix in (24) using Karhunen-Loeve Transform (KLT) [30]. The correlation matrix \mathbf{P} calculated by (24) is a symmetric, positive semi-definite matrix. Let

$$\mathbf{U} \mathbf{D} \mathbf{U}^T = \text{SVD}(\mathbf{P}) \quad (30)$$

denotes the Singular Value Decomposition (SVD) of \mathbf{P} , where columns of \mathbf{U} are the eigenvectors of \mathbf{P} and \mathbf{D} is a diagonal matrix with $\mathbf{d} = \text{diag}(\mathbf{D})$ being the descending ordered eigenvalues of \mathbf{P} . It have been shown in [31] that the basis vectors of a Discrete Cosine Transform (DCT) approach to the eigenvectors of the inverse of an AR(1) matrix as the coefficient r goes to 1. More precisely, from (27) we define

$$\mathbf{K} \triangleq \mathbf{P}^{-1} (1-r^2), \quad (31)$$

then the rows of a DCT Type-2 matrix is the eigenvectors of \mathbf{K} as $r \rightarrow 1$. This property of DCT has made it a popular transform for decomposition of highly correlated signal sources [30].

From (24), (30) and (31), we may regularize the correlation matrix \mathbf{P} with an AR(1) matrix by simply substituting the eigenvalue matrix \mathbf{U} in (30) with a DCT Type-2 matrix,

$$\tilde{\mathbf{P}} = \text{dctmtx}(N)^T \mathbf{D} \text{dctmtx}(N) \quad (32)$$

where $\text{dctmtx}(N)$ generates a DCT Type-2 matrix of size N . We then normalize the diagonal entries of $\tilde{\mathbf{P}}$ to 1s by

$$\mathbf{v} = \sqrt{\text{diag}(\tilde{\mathbf{P}})}, \quad \bar{\mathbf{P}} = \text{diag}^{-1}(\mathbf{v})\tilde{\mathbf{P}}\text{diag}^{-1}(\mathbf{v}) \quad (33)$$

where $\text{diag}^{-1}(\mathbf{v})$ builds a diagonal matrix with the diagonal entries given by \mathbf{v} . In (33), $\bar{\mathbf{P}}$ was the AR(1) approximation to the correlation matrix \mathbf{P} .

γ was updated afterwards using the regularized $\bar{\mathbf{P}}$,

$$\gamma = \frac{1}{N} \text{Tr} [\bar{\mathbf{P}}^{-1}(\boldsymbol{\Sigma} + \boldsymbol{\mu}\boldsymbol{\mu}^T)] \quad (34)$$

Remark 4: Using KLT to exploit the correlation structure in signals has long been exist in literature. In [30], the author studied the use of Toeplitz matrix to approximate empirical correlation matrix. To our best knowledge, our work was the first to use KLT in regularized least squares to solve under-determined optimization problems. The DCT approximation in (32) is also attractive for its computational efficiency in calculating $\boldsymbol{\mu}$, $\boldsymbol{\Sigma}$ and γ in (19), (20) and (34).

4) *Estimate The Quantization Error e (Outer-E Step):* We calculate the expected value of \mathbf{e} from

$$\hat{\mathbf{e}} = E[\mathbf{e} | \mathbf{e} \in \mathcal{D}_e] = \int_{-\Delta/2}^{\Delta/2} \mathbf{e} p(\mathbf{e} | \mathbf{z}, \mathbf{x}; \lambda) d\mathbf{e}$$

which is the expected value of a truncated Normal distribution. $\hat{\mathbf{e}}$ can be obtained analytically [19],

$$\hat{\mathbf{e}} = \boldsymbol{\mu}_e - \sqrt{\lambda} \cdot \frac{\text{PDF}(\mathbf{l}_e) - \text{PDF}(\mathbf{u}_e)}{\text{CDF}(\mathbf{l}_e) - \text{CDF}(\mathbf{u}_e)} \quad (35)$$

where $\boldsymbol{\mu}_e = \mathbf{z} - \boldsymbol{\Phi}\boldsymbol{\mu}_x$, $\mathbf{l}_e = (-\Delta/2 - \boldsymbol{\mu}_e)/\sqrt{\lambda}$ and $\mathbf{u}_e = (\Delta/2 - \boldsymbol{\mu}_e)/\sqrt{\lambda}$. $\text{PDF}(\cdot)$ and $\text{CDF}(\cdot)$ are the probability density function (PDF) and cumulative density function (CDF) of a standard Normal distribution respectively.

Remark 5: Besides the quantization cell width Δ , we may also have the prior information of the reference voltage V_{ref} . For the estimates of the measurements $\hat{\mathbf{z}} = \boldsymbol{\Phi}\boldsymbol{\mu}_x$, values larger than V_{ref} might indicate that saturation occurs. In this case, we may write (35) as,

$$\hat{\mathbf{e}}_{\mathcal{I}} = \boldsymbol{\mu}_{e\mathcal{I}} - \sqrt{\lambda} \cdot \frac{\text{PDF}(\mathbf{l}_{e\mathcal{I}})}{\text{CDF}(\mathbf{l}_{e\mathcal{I}}) - 1} \quad (36)$$

where \mathcal{I} denotes the set of index where $\hat{\mathbf{z}} > V_{ref}$.

5) *The proposed algorithm:* The resulting algorithm is summarized in Fig. 6, named as the Bayesian De-Quantize algorithm (**BDQ**).

Remark 6: The **BDQ** algorithm can be used to recover piecewise smooth signals from quantized, and possibly under-determined measurements. It shares some similarities with the Block Sparse Bayesian Learning (BSBL) framework [14] in non-sparse mode where only the correlations within signals are exploited. However, in the experiment we found that the regularization method (32)-(33) on \mathbf{P} in **BDQ** was superior to the empirical methods in BSBL, which yielded better recovery results on physiological signals.

```

1: procedure BDQ( $\mathbf{z}, \boldsymbol{\Phi}$ )
2:   Outputs:  $\mathbf{x}, \mathbf{e}$ 
3:   Initialize:  $\gamma = 1, \mathbf{P} = \mathbf{I}, \lambda = 0.001$ 
4:   while not converged do
5:     Estimate  $\boldsymbol{\mu}, \boldsymbol{\Sigma}$  by (19), (20).
6:     Calculate  $\mathbf{P}$  via (24)
7:     Regularize  $\bar{\mathbf{P}}$  via (32)-(33).
8:     Calculate  $\gamma$  via (34).
9:     Calculate  $\hat{\mathbf{e}}$  by (35)
10:    Update  $\mathbf{y} = \mathbf{z} - \hat{\mathbf{e}}$ 
11:   end while
12: end procedure

```

Fig. 6. The Bayesian De-Quantize (BDQ) algorithm.

IV. EXPERIMENTS AND RESULTS

A. Datasets

We simultaneously collected ECG, PPG and accelerometer signals from 12 volunteers with age ranged from 18 to 35. Fig. 7 shows the hardware set up for data recording. For

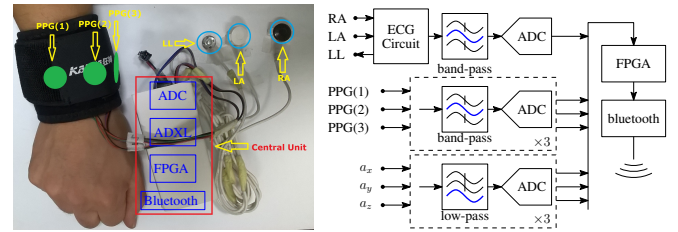


Fig. 7. The hardware setup for data recording. ECG, PPG and accelerometer signals were simultaneously collected. Wet electrodes were used to obtain a three-lead ECG, where the leads LA and RA were placed at left and right chest respectively, and the LL lead was placed at the left lower abdomen. PPG signals were collected using reflective pulse oximeter sensors with green LED (wavelength: 515nm). Two PPG sensors were placed at the back of the wrist while another one was placed right on the pulse position. Three axial accelerometer data were collected using ADXL345 with $\pm 4g$ range. Data were transmitted to a laptop via bluetooth.

each subject, we recorded data for 5 ~ 6 minutes. During data collection, a subject ran on a treadmill with speeds ranged from 2km/hour to 15km/hour. The sensor band was conveniently worn on the wrist and we intentionally introduced additional artifacts by asking all subjects to pull clothes, wipe sweat, swig arms during data recording.

All signals were filtered and then sampled at 125Hz with 12 bits precision per sample. Table I shows the specifications for all analog filters.

TABLE I
SPECIFICATIONS FOR ANALOG FILTERS. f_{c1} AND f_{c2} DENOTE THE LOWER AND UPPER CUTOFF FREQUENCIES AT 22DB ATTENUATION.

	ECG	PPG	Accelerometer
Filter Type	Band-pass	Band-pass	Low-pass
f_{c1}	0.1Hz	0.25Hz	-
f_{c2}	100Hz	14.5Hz	100Hz

In the simulation framework, ECG signals were only used as reference signals to extract the ground truth heart rate. One

channel PPG (site PPG(1) placed at the back of the wrist) and three-axis accelerometer were the data actually used. We downsampled (Nyquist sampling) PPG and accelerometer signals to 31.75Hz in the experiments. It should be noted that the accelerometer data contained aliasing when downsampled at 31.75Hz. However, such distortions were small as the rate of most activities during fitness training rarely exceed 10Hz.

B. Experiments Setup

Fig. 8 shows the experiment setup. Quantized compressed

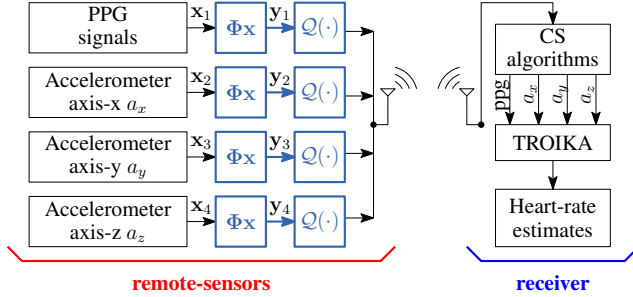


Fig. 8. The quantized compressed sensing was applied on PPG and three axial accelerometer data to reduce the transmission bit-budget. At the receiver, data were recovered from quantized measurements, and the TROIKA framework was applied on the recovered data to estimate the heart rate.

sensing is applied on PPG and accelerometer signals. Raw segments $\{x_1, x_2, x_3, x_4\}$ from each data channel are compressed by $y = \Phi x$ simultaneously. Sparse binary sensing matrices, whose entries consisted of only 0s and 1s, are used in the experiment. Such matrix preserves low-power property when implemented in FPGA [10]. We fix each column of Φ consisting exactly 2 non-zero entries and also make sure Φ is full row-rank in each iteration. The compressed measurements $\{y_1, y_2, y_3, y_4\}$ are further quantized by $Q(\cdot)$ to reduce the transmission bit-budget.

At the receiver, CS algorithms are used to recover signals from quantized measurements. The heart rate is estimated by the TROIKA [32] framework using the recovered PPG and accelerometer datasets.

The codes and data reproducing the results in the experiments are available at <https://github.com/liubenyanu/qsbl>.

C. Performance Measurement

We use two performance metrics. One is the reconstruction SNR (RSNR),

$$\text{RSNR (dB)} = 10 \log_{10} \frac{\|\mathbf{x}\|_2^2}{\|\hat{\mathbf{x}} - \mathbf{x}\|_2^2}$$

where $\hat{\mathbf{x}}$ denotes the recovered signal of \mathbf{x} . To assess the averaged performance over all segments, we refer to the average RSNR (ARSNR), defined by

$$\text{ARSNR (dB)} = 10 \log_{10} \frac{1}{S} \sum_{i=1}^S \left(\frac{\|\mathbf{x}_i\|_2^2}{\|\hat{\mathbf{x}}_i - \mathbf{x}_i\|_2^2} \right) \quad (37)$$

where \mathbf{x}_i is the i th signal segment and S is the total number of segments in a dataset. The second metric is the Structural

Similarity index (SSIM) [33]. SSIM measures the similarity between recovered signals and original signals, which is a better metric than RSNR [15], [33].

The qualities of recovery are not only characterized by RSNR, but also by application specific requirements. Therefore, we perform a task-driven approach where the heart rate estimates from the recovered PPG and accelerometer signals are evaluated. The average absolute estimation error (Error1), defined in [32], was,

$$\text{Error1} = \frac{1}{W} \sum_{i=1}^W |\text{BMP}_{\text{est}}(i) - \text{BMP}_{\text{true}}(i)| \quad (38)$$

where W is the total number of heart rate estimates, $\text{BMP}_{\text{est}}(i)$ is the estimated heart rate in the i th time window¹ and $\text{BMP}_{\text{true}}(i)$ is the ground truth heart rate. The standard deviation of heart rate estimates, denoted by SD_{BPM} , is

$$\text{SD}_{\text{BPM}} = \sqrt{\frac{1}{W} \sum_{i=1}^W (\text{BMP}_{\text{est}}(i) - \text{BMP}_{\text{true}}(i))^2} \quad (39)$$

Pearson correlation between the ground-truth and the heart rate estimates is also calculated for comparison.

D. The Recovery Algorithms for Quantized CS

Besides the proposed algorithm, we use the following two typical CS algorithms: QVMP [19] and BSBL-BO [3].

(1) **QVMP [19]**. QVMP is a variational Bayesian De-Quantization algorithm proposed in [19]. As shown in [19], it has better performance than QIHT [18] and L1RML [17]. However, QVMP can not recover physiological signals directly in time domain. Instead, we applied QVMP in transformed domain, where

$$\mathbf{z} = (\Phi \Psi) \boldsymbol{\theta} + \mathbf{e} + \mathbf{n}$$

Ψ is a sparse representation matrix and $\boldsymbol{\theta}$ is the sparse coefficients. QVMP firstly recovered $\hat{\boldsymbol{\theta}}$, then $\hat{\mathbf{x}}$ via $\hat{\mathbf{x}} = \Psi \hat{\boldsymbol{\theta}}$.

In the experiment, Discrete Cosine Transform (DCT) matrix was selected for Ψ and we set $\lambda = 0.001/M$, $\text{tol} = 1e^{-6}$, $\text{maxiter} = 400$ for QVMP as it achieved best recovery performance on the datasets.

(2) **BSBL-BO [3], [14]**. BSBL-BO [14] is the best performing CS algorithm in recovering physiological signals such as fetal ECG [3] or EEG [15]. In the experiment, we observed that BSBL-BO can also recover signals from quantized measurements, by modeling quantization errors using a zero mean Normal distribution with a larger variance λ_e .

Throughout the experiment, BSBL-BO worked in non-sparse mode and directly recovered signals in time domain. We selected $\text{blkLen} = 32$, $\text{LearnLambda} = 2$, $\text{maxiter} = 64$ and $\text{LearnType} = 1$ for BSBL-BO as this setting achieved best recovery performance. The recoveries of BSBL-BO using real-valued measurement were also calculated, where the parameter $\text{LearnLambda} = 0$ was used.

¹The TROIKA algorithm [32] operates in a sliding window manner. A time window of T seconds is sliding on the signals with incremental step S seconds, and the heart rate estimates are based on the samples collected within this time window. We use default parameters ($T = 8s$, $S = 2s$) for TROIKA in our experiments.

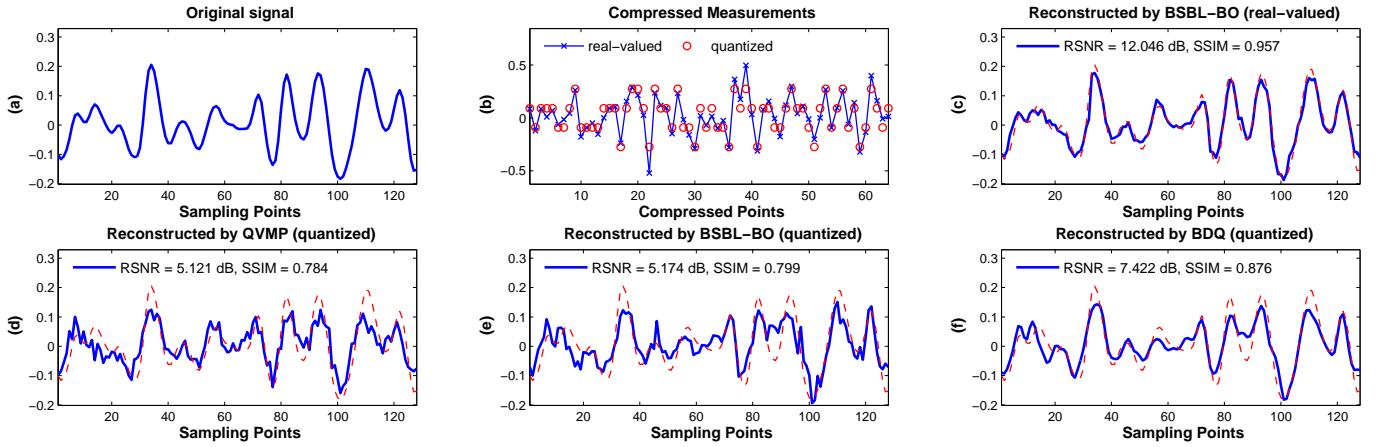


Fig. 9. Performances of different CS algorithms on quantized measurements. (a) a raw PPG segment \mathbf{x} was collected in 4s ($N = 128$). (b) real-valued compressed measurements ($M = 64$, $CR = 0.50$) were generated via $\mathbf{y} = \Phi\mathbf{x}$ and then quantized by $\mathcal{Q}(\cdot)$ with 2 bits per measurement. The transmission bit-budget was only $MB = 128$ bits. (c) on real-valued measurements, BSBL-BO recovered original signals with $RSNR = 12.046$ dB and $SSIM = 0.957$. (d) QVMP recovered signals in DCT domain with $RSNR = 5.121$ dB and $SSIM = 0.784$. (e)(f) BSBL-BO and BDQ recovered signals directly in time domain with $RSNR = 5.174$ dB, $SSIM = 0.799$ and $RSNR = 7.422$ dB, $SSIM = 0.876$ respectively.

E. Results

1) *An illustrative example:* To better understand the quantized compressed sensing and the quality of signal recovery using different CS algorithms, an illustrative example was given in Fig. 9.

- 1) Fig. 9 (a). A raw PPG segment \mathbf{x} of size $N = 128$ was shown. In our experiments, signals were divided into fixed-sized segments and each segment was normalized (i.e., $\mathbf{x}/\|\mathbf{x}\|$) before compression.
- 2) Fig. 9 (b). A segment \mathbf{x} was compressed via CS, $\mathbf{y} = \Phi\mathbf{x}$, where Φ was a sparse binary matrix with $M = 64$ rows and the compression ratio $CR = 0.50$. The compressed measurements were further quantized by $\mathcal{Q}(\cdot)$ with $B = 2$ bits per measurement. The reference voltage for the quantizer was $V_{ref} = 0.70 \max(\mathbf{y})$. The quantized measurements $\mathbf{z} = \mathcal{Q}(\mathbf{y})$ have only 4 finite values and contain saturations. The total transmission bit-budget was only $MB = 128$ bits.
- 3) Fig. 9 (c) shows the recovery results of BSBL-BO using real-valued measurements \mathbf{y} .
- 4) Fig. 9 (d)(e)(f) shows the recovery results of QVMP, BSBL-BO and BDQ using the quantized measurements \mathbf{z} . QVMP and BDQ used the prior information of quantization cell width Δ to assist recovery.

Using the same settings in Fig. 9, we presented ARSNR and SSIM of different types of signals on the dataset ‘subject-02’ in Fig. 10. The ARSNR was calculated on all 74 segments in this dataset. The results in Fig. 9 and Fig. 10 shows that the proposed algorithm, BDQ, yielded better signal recoveries from quantized measurements than QVMP and BSBL-BO.

We also presented results in recovering PPG signals using multiple quantization bit-depth $B \in \{2, 3, 4, 6, 8\}$ in Fig. 11. The proposed algorithm, BDQ, was in average 1.640dB superior to BSBL-BO and 3.547dB to QVMP. Both BDQ and BSBL-BO were superior to QVMP.

For larger bit-depth B such as $B \in \{6, 8\}$, the variance of the quantization error is small and can be approximated

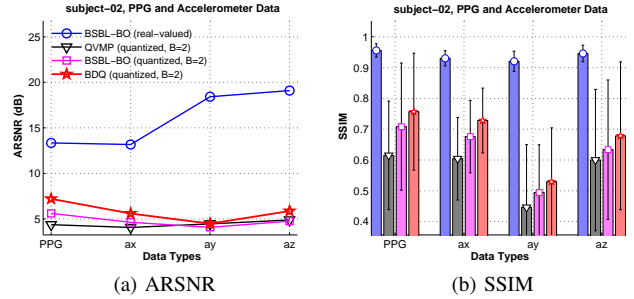


Fig. 10. The ARSNR and SSIM of signal recoveries w.r.t different types of signals. The parameters $N = 128$, $M = 64$, $B = 2$ were used. The three-axial accelerometer data were denoted by ax (x-axis), ay (y-axis) and az (z-axis) respectively.

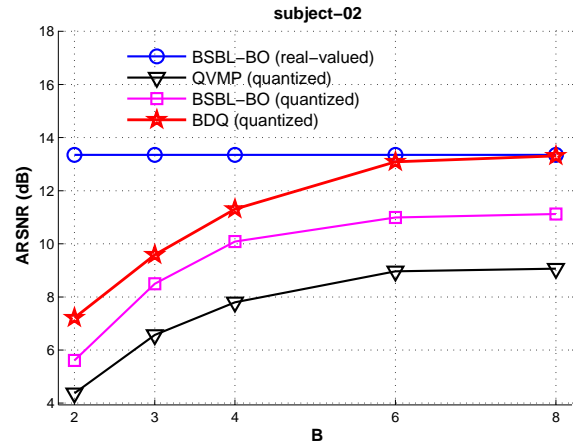


Fig. 11. The ARSNR in recovering PPG signals in dataset ‘subject-02’ with multiple quantization bit-depth B .

by a Normal distribution. However, in Fig. 11, we observed performance gap between BSBL-BO (real-valued) and BSBL-BO (quantized) when $B \in \{6, 8\}$. This was largely caused by the saturation errors of the quantizer, whose distributions

are unbounded and can not be approximated by a Normal distribution. In contrast, BDQ yielded similar recovery performance to BSBL-BO (real-valued) when $B \in \{6, 8\}$. The reasons were two-fold, one was that the regularization (32)-(33) on the correlation matrix in BDQ can better exploit the highly correlated structure in PPG signals than the empirical method used in BSBL-BO, the other was the learning rules (35) for quantization errors can account for mild saturations introduced by the quantizer.

2) *The trade-off between the compression of CS and the quantization bit-depth:* Quantized CS, when applied to data compression for low-energy telemonitoring, is basically a two-stage compressor. Firstly, we compress a raw segment of N samples via compressed sensing to achieve a preliminary compression ratio $CR = (N - M)/N$. Then the measurements are efficiently encoded by quantization with only B bits per measurement to further reduce the transmission bit-budget.

We present in Fig. 12 the results with varying number of measurements $M \in \{32, 64, 96\}$ and quantization bit-depth $B \in \{2, 3, 4, 6, 8\}$. We also present results of traditional

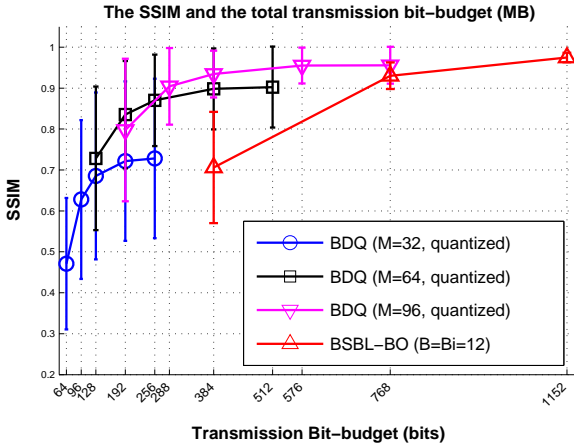


Fig. 12. The SSIM w.r.t different transmission bit-budget MB in recovering the PPG channel of dataset ‘subject-02’. We fixed $N = 128$ and varied $M \in \{32, 64, 96\}$. BDQ was used to recover signals from quantized measurements with different bit-depth B .

sample-based compression using BSBL-BO, where the bits per compressed measurement is equal to the bit-depth of the signals in the dataset, i.e., $B = B_i = 12$. Fig. 13 shows the absolute heart rate estimation error (Error1) and SD_{BPM} with respect to different transmission bit-budget.

From the results in Fig. 12 and Fig. 13, we found that both the SSIM and Error1 are affected by the configurations of M and B even if under the same transmission bit-budget. In fact, CS provides random mixing of signals to compressed measurements, each compressed measurement preserves information on original signals while the quantization process drops information. Therefore, if we were going to quantize the compressed measurements with small bit-depth B , the compression ratio CR can not be high. In Fig. 13, the configuration $M = 64$ had the minimal Error1 for $MB < 512$ bits. It is worth noting that smaller values of MB is always preferable since it reduces total transmission bit-budget. For $N = 128, B_i = 12$ and the optimal configuration (point A

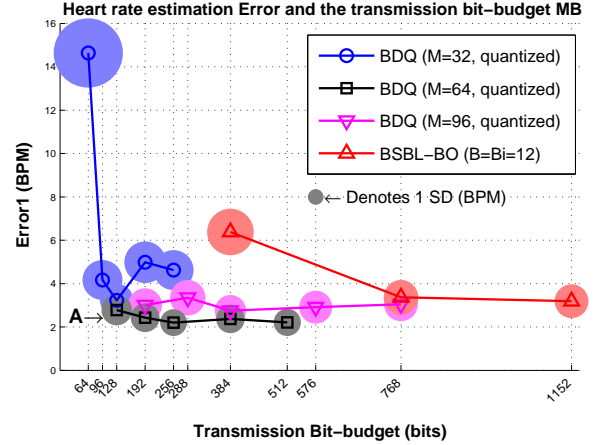


Fig. 13. The heart rate estimation error (Error1) and SD_{BPM} w.r.t different transmission bit-budget MB . For each configuration (M, B) , the diameter of a solid circle is proportional to the SD_{BPM} metric of this configuration. Point A denotes the optimal configuration where $M = 64$ and $B = 2$.

in Figure. 13) of quantized CS $M = 64, B = 2$, the bit compression ratio CR_b , defined in (14), is

$$CR_b = \frac{NB_i - MB}{NB_i} = 1 - 0.50 \cdot \frac{2}{12} = 0.9167.$$

We achieved 91.67% bit compression ratio and transmitted 128 bits instead of 128 samples for telemonitoring.

3) *Heart rate estimates from recovered datasets:* We now presented results on the whole datasets using the optimal configurations of quantized CS with $N = 128, M = 64, CR = 0.50$ and $B = 2$. Fig. 14 shows the absolute error (Error1) per subject, Table II lists absolute error (Error1), Standard Deviation (SD_{BPM}) and Pearson correlation calculated over all subjects. By jointly using the optimal configuration for quantized CS and the proposed algorithm, we achieved $Error1 = 2.596$ (BPM), $SD_{BPM} = 3.625$ (BPM) and 0.9899 Pearson correlation, which is closely to the result on non-compressed datasets. The results in Table. II also shows that for signal recovery from quantized measurements, BDQ was superior to both QVMP and BSBL-BO.

The Scatter Plot between the ground-truth heart rates and the estimates using the recovered datasets is shown in Fig. 15. The fitted line for BSBL-BO ($CR = 0.50, B = 2$) and BDQ ($CR = 0.50, B = 2$) was $y = 0.999x - 0.866, (R^2 = 0.960)$ and $y = 1.002x - 1.333, (R^2 = 0.980)$ respectively, where x indicates the ground-truth heart rate value and y is the estimates from recovered data, R^2 is a measure for goodness of linear fit.

V. DISCUSSIONS

A. The quantizer $\mathcal{Q}(\cdot)$

The performance of signal recovery from quantized measurements clearly depends on the choice of the quantizer. For the uniform quantizer used in this paper, the dilemma is the choice of reference voltages V_{ref} .

In our experiments, signal \mathbf{x} was normalized via $\mathbf{x}/\|\mathbf{x}\|$ and then compressed by $\mathbf{y} = \Phi\mathbf{x}$, the reference voltage V_{ref} for

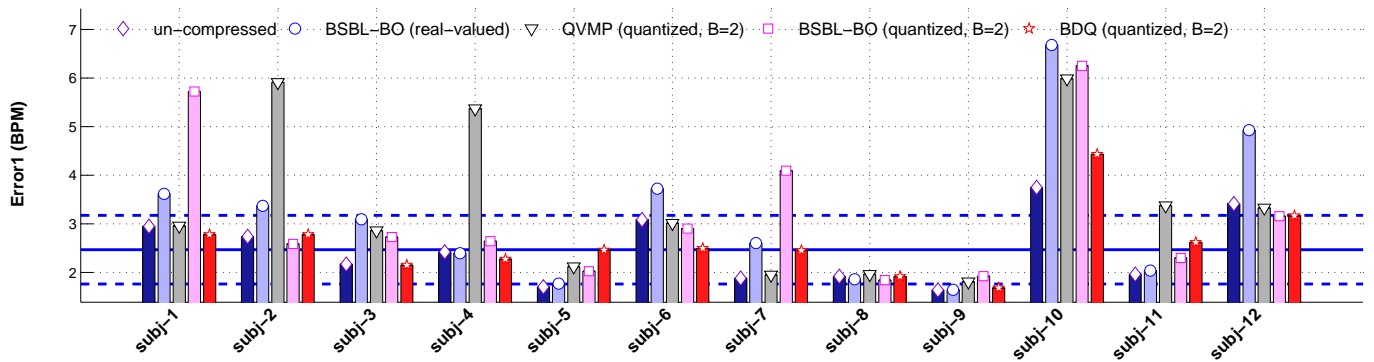
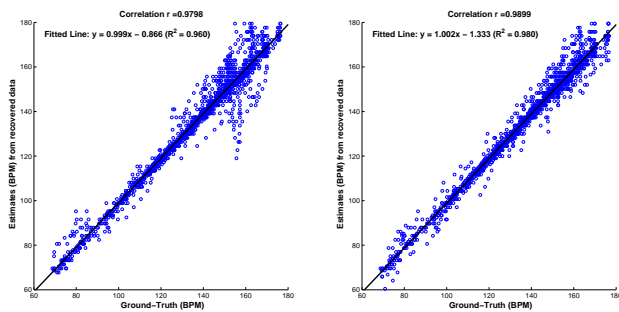


Fig. 14. The absolute heart rate estimation error (Error1) on each subject using non-compressed datasets (denoted by ‘un-compressed’) and the recovered datasets by different CS algorithms. The solid and the dashed line denote mean \pm standard deviation of Error1 averaged over all subjects using non-compressed datasets. Using the optimal configuration of the quantized CS ($N = 128$, $M = 64$, $CR = 0.50$, $B = 2$) and the proposed BDQ algorithm, we achieved stable and closely performance to that of ‘un-compressed’.

TABLE II
THE AVERAGED ERROR1 AND THE PEARSON CORRELATION OVER ALL 12 SUBJECTS.

	Uncompressed	Quantized CS ($CR = 0.50$, $B = 2$)			
		Real-valued CS BSBL-BO	QVMP	BSBL-BO	BDQ
Error1 (BPM)	2.464	3.137	3.355	3.179	2.596
SD_{BPM} (BPM)	3.554	5.022	5.561	5.030	3.625
Pearson Correlation r	0.9902	0.9810	0.9747	0.9798	0.9899



(a) BSBL-BO ($CR = 0.50$, $B = 2$) (b) BDQ ($CR = 0.50$, $B = 2$)

Fig. 15. Scatter Plot between the ground-truth heart rate and the estimates using the recovered data by BSBL-BO ($CR = 0.50$, $B = 2$) and BDQ ($CR = 0.50$, $B = 2$). The Pearson correlation was 0.9798 and 0.9899 for BSBL-BO and BDQ respectively. The ‘Fitted Line’ is the linear fit of the estimates to ground-truth heart rate. The R^2 value, which is an estimates for goodness of linear fit, was 0.960 for BSBL-BO and 0.980 for BDQ.

the quantizer $\mathcal{Q}(\cdot)$ was set to $V_{ref} = 0.70 \max(\mathbf{y})$. It is worth noting that $V_{ref} = 0.70 \max(\mathbf{y})$ is not the optimal reference voltage for this datasets and we do not search for such optimal values to avoid overfitting. However one should take care that for smaller values of V_{ref} there may be more saturations, while for larger values of V_{ref} there may be more underflows.

At the first sight, signal normalization $\mathbf{x}/\|\mathbf{x}\|$ and $\max(\mathbf{y})$ are not practical for implementing in hardware and also for low energy applications. Instead, this problem is solvable by instead fixing the reference voltage for an ADC and using an Automatic Gain Control (AGC) circuit to tune the scale of signals in between $[-V_{ref}, V_{ref}]$. The gains of AGC must be transmitted alongside with the compressed bits for signal

recovery.

B. Signal recovery directly in the time domain

In literature most CS algorithms recover signals in a transform domain Ψ where signals \mathbf{x} can be sparsely represented. By suitably choosing the transformation matrix, one can improve the quality of recovery.

However, in practice, physiological signals recorded by wearable devices are usually contaminated by various strong artifacts, such as artifacts due to body motion and hardware issues [3], [23]. As a result, many of these signals are less sparse in many known transform domains. Seeking/designing an optimal transformation matrix for a specific kind of physiological signals may be difficult. In this situation, recovering the signals from transform domains is not effective. In [3], BSBL-BO was used to recover raw fetal ECG recordings directly in the time domain by exploiting temporal correlations of these recordings, revealing that exploiting correlations of signals is an alternative method to exploiting sparsity. An obvious advantage of this method is that it avoids the seeking of an optimal transformation matrix for recovery. Our proposed BDQ algorithm also suggested the effectiveness of this method.

C. Quantized CS as data encoders for more types of signals

The CS and the quantizer are analogue to the Discrete Wavelet Transform (DWT) and the scalar quantization unit used in the JPEG standard [34]. However, CS can be low-energy implemented in FPGA [10] and the additional 2-bit quantizer barely consumes any resource using fix-point arithmetic [10]. The data compressor proposed in this work

can be used as a low-energy data compressor/encoder for potentially more types of signals such as audios or images.

VI. CONCLUSIONS

In this paper, we present an approach for low-energy wireless telemonitoring using quantized compressed sensing. The contributions of this paper are two-fold. First, we propose a two-stage data compressor, where signals are compressed by CS with a compression ratio $CR = 0.50$ and then quantized with $B = 2$ bits per measurement. Second, to pursue better signal recoveries from quantized measurements, we develop a Bayesian de-quantization algorithm that can exploit both the model of quantization errors and the correlated structure within signals. Experiment results showed that, by jointly using the proposed data compressor and the recovery algorithm, we achieved 2.596 absolute heart rate estimation errors and 0.9899 Pearson correlation on whole datasets, which was closely to the performance on non-compressed datasets. The results imply that we can effectively transmit N bits instead of N samples, which may revolution the way we compress data for low-energy wireless telemonitoring.

REFERENCES

- [1] C. A. Meier, M. C. Fitzgerald, and J. M. Smith, "ehealth: Extending, enhancing, and evolving health care," *Annual review of biomedical engineering*, vol. 15, pp. 359–382, 2013.
- [2] E. Candes and M. Wakin, "An introduction to compressive sampling," *Signal Processing Magazine, IEEE*, vol. 25, no. 2, pp. 21–30, march 2008.
- [3] Z. Zhang, T.-P. Jung, S. Makeig, and B. Rao, "Compressed sensing for energy-efficient wireless telemonitoring of noninvasive fetal ECG via block sparse bayesian learning," *Biomedical Engineering, IEEE Transactions on*, vol. 60, no. 2, pp. 300–309, 2013.
- [4] D. Craven, B. McGinley, L. Kilmartin, M. Glavin, and E. Jones, "Compressed sensing for bioelectric signals: A review," *Biomedical and Health Informatics, IEEE Journal of*, vol. PP, no. 99, pp. 1–1, 2014.
- [5] F. Chen, A. Chandrakasan, and V. Stojanovic, "Design and analysis of a hardware-efficient compressed sensing architecture for data compression in wireless sensors," *Solid-State Circuits, IEEE Journal of*, vol. 47, no. 3, pp. 744–756, 2012.
- [6] F. Chen, F. Lim, O. Abari, A. Chandrakasan, and V. Stojanovic, "Energy-aware design of compressed sensing systems for wireless sensors under performance and reliability constraints," *Circuits and Systems I: Regular Papers, IEEE Transactions on*, vol. 60, no. 3, pp. 650–661, 2013.
- [7] J. Haboba, M. Mangia, F. Pareschi, R. Rovatti, and G. Setti, "A pragmatic look at some compressive sensing architectures with saturation and quantization," *Emerging and Selected Topics in Circuits and Systems, IEEE Journal on*, vol. 2, no. 3, pp. 443–459, 2012.
- [8] A. Wang, W. Xu, Z. Jin, and F. Gong, "Quantization effects in an analog-to-information front-end in eeg tele-monitoring," *Circuits and Systems II: Express Briefs, IEEE Transactions on*, vol. PP, no. 99, pp. 1–1, 2015.
- [9] H. Mamaghanian, N. Khaled, D. Atienza, and P. Vandergheynst, "Compressed sensing for real-time energy-efficient ECG compression on wireless body sensor nodes," *Biomedical Engineering, IEEE Transactions on*, vol. 58, no. 9, pp. 2456–2466, 2011.
- [10] B. Liu, Z. Zhang, G. Xu, H. Fan, and Q. Fu, "Energy efficient telemonitoring of physiological signals via compressed sensing: A fast algorithm and power consumption evaluation," *Biomedical Signal Processing and Control*, vol. 11C, pp. 80–88, 2014.
- [11] S. Becker, J. Bobin, and E. Candes, "Nesta: a fast and accurate first-order method for sparse recovery," *SIAM Journal on Imaging Sciences*, vol. 4, no. 1, pp. 1–39, 2011.
- [12] R. G. Baraniuk, V. Cevher, M. F. Duarte, and C. Hegde, "Model-based compressive sensing," *IEEE Transactions on Signal Processing*, vol. 56 (4), pp. 1982–2001, 2010.
- [13] J. Pant and S. Krishnan, "Compressive sensing of electrocardiogram signals by promoting sparsity on the second-order difference and by using dictionary learning," *IEEE transactions on biomedical circuits and systems*, vol. 8, no. 2, pp. 293–302, 2014.
- [14] Z. Zhang and B. Rao, "Extension of SBL algorithms for the recovery of block sparse signals with intra-block correlation," *Signal Processing, IEEE Transactions on*, vol. 61, no. 8, pp. 2009–2015, 2013.
- [15] Z. Zhang, T.-P. Jung, S. Makeig, and B. Rao, "Compressed sensing of EEG for wireless telemonitoring with low energy consumption and inexpensive hardware," *Biomedical Engineering, IEEE Transactions on*, vol. 60, no. 1, pp. 221–224, 2013.
- [16] R. M. Gray and D. L. Neuhoff, "Quantization," *IEEE Trans. Info. Theory*, vol. 44, no. 6, pp. 1–63, 1998.
- [17] A. Zymnis, S. Boyd, and E. Candes, "Compressed Sensing With Quantized Measurements," *IEEE Transaction on Signal Processing*, vol. 17, no. 2, pp. 149–152, 2010.
- [18] L. Jacques, K. Degraux, and C. De Vleeschouwer, "Quantized iterative hard thresholding: Bridging 1-bit and high-resolution quantized compressed sensing," *arXiv preprint arXiv:1305.1786*, 2013. [Online]. Available: <http://perso.uclouvain.be/laurent.jacques/index.php/Main/QIHTDemo>
- [19] Z. Yang, L. Xie, and C. Zhang, "Variational bayesian algorithm for quantized compressed sensing," *Signal Processing, IEEE Transactions on*, vol. 61, no. 11, pp. 2815–2824, June 2013.
- [20] L. Jacques, D. K. Hammond, and M.-J. Fadili, "Dequantizing compressed sensing: When oversampling and non-gaussian constraints combine," *IEEE Transactions on Information Theory*, vol. 57, no. 1, pp. 559–571, 2011.
- [21] V. Cambareri, M. Mangia, F. Pareschi, R. Rovatti, and G. Setti, "Low-complexity multiclass encryption by compressed sensing, part i: Definition and main properties," *arXiv preprint arXiv:1307.3360*, 2013.
- [22] J. Laska, P. Boufounos, M. Davenport, and R. Baraniuk, "Democracy in action: Quantization, saturation, and compressive sensing," *Applied and Computational Harmonic Analysis*, vol. 31, no. 3, pp. 429–443, 2011.
- [23] Z. Zhang, B. D. Rao, and T.-P. Jung, "Compressed sensing for energy-efficient wireless telemonitoring: Challenges and opportunities," in *Asilomar Conference on Signals, Systems and Computers (Asilomar 2013)*, 2013.
- [24] D. A. Van Dyk, "Nesting em algorithms for computational efficiency," *Statistica Sinica*, vol. 10, no. 1, pp. 203–226, 2000.
- [25] R. Prasad, C. R. Murthy, and B. D. Rao, "Nested sparse bayesian learning for block-sparse signals with intra-block correlation," in *Acoustics, Speech and Signal Processing (ICASSP), 2014 IEEE International Conference on*. IEEE, 2014, pp. 7183–7187.
- [26] M. E. Tipping, "Sparse bayesian learning and the relevance vector machine," *Journal of Machine Learning Research*, vol. 1, pp. 211–244, 2001.
- [27] Z. Zhang and B. D. Rao, "Sparse signal recovery with temporally correlated source vectors using sparse bayesian learning," *IEEE Journal of Selected Topics in Signal Processing*, vol. 5, no. 5, pp. 912–926, 2011.
- [28] J. Zhou, L. Yuan, J. Liu, and J. Ye, "A multi-task learning formulation for predicting disease progression," in *Proceedings of the 17th ACM SIGKDD international conference on Knowledge discovery and data mining*. ACM, 2011, pp. 814–822.
- [29] S. D. Babacan, S. Nakajima, and M. N. Do, "Bayesian group-sparse modeling and variational inference," *Submitted to IEEE Transactions on Signal Processing*, 2012.
- [30] A. N. Akansu and M. U. Torun, "Toeplitz approximation to empirical correlation matrix of asset returns: A signal processing perspective," *Selected Topics in Signal Processing, IEEE Journal of*, vol. 6, no. 4, pp. 319–326, 2012.
- [31] G. Strang, "The discrete cosine transform," *SIAM review*, vol. 41, no. 1, pp. 135–147, 1999.
- [32] Z. Zhang, Z. Pi, and B. Liu, "TROIKA: A General Framework for Heart Rate Monitoring Using Wrist-Type Photoplethysmographic Signals During Intensive Physical Exercise," *IEEE Transactions on Biomedical Engineering*, vol. 62, no. 2, pp. 522 – 531, 2015.
- [33] Z. Wang and A. Bovik, "Mean squared error : Love it or leave it ? a new look at signal fidelity measures." *IEEE Signal Processing Magazine*, vol. 26 (1), pp. 98–117, 2009.
- [34] A. Skodras, C. Christopoulos, and T. Ebrahimi, "The jpeg 2000 still image compression standard," *Signal Processing Magazine, IEEE*, vol. 18, no. 5, pp. 36–58, 2001.